Reactivity of $Cr^+(^6S,^4D)$, $Mn^+(^7S,^5S)$, and $Fe^+(^6D,^4F)$: Reaction of Cr^+, Mn^+, and Fe^+ with Water

Arantxa Irigoras, Joseph E. Fowler, and Jesus M. Ugalde*

Contribution from the Kimika Fakultatea, Euskal Herriko Unibertsitatea, P.K. 1072, 20080 Donostia, Euskadi, Spain

Received December 31, 1998. Revised Manuscript Received June 17, 1999

Abstract: The study of the reaction of water with the first-row transition-metal ions is continued in this work. Here we report the study of the reaction of water with the middle (Cr^+, Mn^+, and Fe^+) first-row transition-metal cations in both high- and low-spin states. In agreement with experimental observations, the oxides are predicted to be more reactive than the metal ions, and no exothermic products are observed. Formation of endothermic products is examined. An in-depth analysis of the reaction paths leading to the observed products is given, including various minima, and several important transition states. All results have been compared with existing experimental and theoretical data, and our earlier works covering the (Sc^+, Ti^+, V^+) + H_2O reactions to observe existent trends for the early first-row transition-metal ions. The $MO^+ + H_2$ energy relative to $M^+ + H_2O$ increases through the series from left to right. Additionally, the Fe^+ case is seen to be significantly different from the entire Sc^+-Mn^+ series because both its low- and high-spin cases involve paired electrons, and Mn^+ shows some differences because of the complete half-filling of its valence shell in the high-spin case.

1. Introduction

The H−H bond activation by MO^+ is a simple system that can be studied in detail both experimentally and theoretically.[1] Thus, it can be used as a model for other reactions of MO^+ with organic substrates. It was pointed out by Armentrout and co-workers that the early transition metal cations (Sc^+, Ti^+, and V^+) are more reactive than their oxides, while the contrary occurs with the middle metals (Cr^+, Mn^+, and Fe^+).[2] Our earlier works[3,4] agreed well with experimental work regarding the reactions of the early transition metals, and here we expand upon those works investigating the middle transition metals to unveil some of the details underlying the observed reversed reactivity.

Indeed, the reactivity of the middle transition metals has been the subject of several earlier investigations. As early as 1986, Kang and Beauchamp[5,6] studied the reactivity of the CrO^+ ion by ion beam reactive scattering techniques. They pointed out that, in comparison with other first-row transition-metal oxides which are either too stable (Sc^+, Ti^+, and V^+) or too reactive (Mn^+, Fe^+, Co^+, and Ni^+), CrO^+ exhibits a balance in being reactive but selective toward olefins. Thus, the chromiun oxide ion undergoes facile reactions with alkanes larger than methane, but not with H_2 or CH_4 even though those reactions are exothermic.

More recently the reactivity of the manganese oxide cation with dihydrogen and alkanes has been studied both experimentaly and theoretically by Ryan et al.[7] They compare results from the Fourier transform ion cyclotron resonance mass spectrometry with those calculated at the CASPT2D level of theory. They found that thermalized MnO^+ reacts very efficiently with H_2 to eliminate either a $H^\bullet$ radical or H_2O from the collision complex, both reactions commencing with H-atom abstraction.

Extensive theoretical and experimental works have been carried out concerning the reactivity of iron with many small molecules. The reactivity of FeO^+ with molecular hydrogen was first studied experimentally by Schröder et al.[8] They found that approximately only 1 in 100 collisions of FeO^+ with H_2 results in product formation. This does not follow simple spin selection rule arguments since the sextet ground state of FeO^+ correlates with the electronic ground state of the product ion $Fe^+(^6D)$, and also the electronic ground state of the $H-Fe^+-OH$ and $Fe(OH_2)^+$ intermediates corresponds to a sextet. Additionally, the symmetry breaking through the approaching H_2 molecule does not violate any spatial symmetry selection rule. The reactive coordination of the hydrogen molecule to FeO^+ was suggested to be at the origin of the barrier of the higher exothermic oxidation of H_2. The most likely pathway in their opinion proceeds via a multicentered coordination to generate the $H-Fe^+-OH$ intermediate:

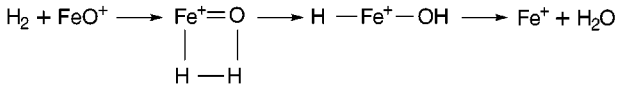

Almost at the same time, Armentrout's group[9] reported on the state-specific reactions of $Fe^+(a^6D,a^4F)$ with D_2O and the

(1) Schröder, D.; Schwarz, H. *Angew. Chem., Int. Ed. Engl.* **1995**, *34*, 1973.
(2) Clemmer, D. E.; Aristov, N.; Armentrout, P. B. *J. Phys. Chem.* **1993**, *97*, 544−552.
(3) Irigoras, A.; Fowler, J. E.; Ugalde, J. M.; *J. Phys. Chem. A* **1998**, *102*, 293; **1998**, *102*, 2252.
(4) Irigoras, A.; Fowler, J. E.; Ugalde, J. M. *J. Am. Chem. Soc.*, in press.
(5) Kang, H.; Beauchamp, J. L. *J. Am. Chem. Soc.* **1986**, *108*, 5663.
(6) Kang, H.; Beauchamp, J. L. *J. Am. Chem. Soc.* **1986**, *108*, 7502.
(7) Ryan, M. F.; Fiedler, A.; Schröder, D.; Schwarz, H. *J. Am. Chem. Soc.* **1995**, *117*, 2033.
(8) Schröder, D.; Fiedler, A.; Ryan, M. F.; Schwarz, H. *J. Phys. Chem.* **1994**, *98*, 68.
(9) Clemmer, D. E.; Chen, Y.-M.; Khan, F. A.; Armentrout, P. B. *J. Phys. Chem.* **1994**, *98*, 6522.

10.1021/ja984469u CCC: $18.00
Published on Web 09/08/1999

reactions of FeO^+ with D_2 as a function of translational energy in a guided ion beam tandem mass spectrometer. The only products observed from single-collision events in the $Fe^+(a^6D,a^4F) + D_2O$ reaction were the endothermic FeD^+ and $FeOD^+$. At low energies, they also observe the $FeOD_2^+$ adduct as a result of secondary stabilizing collisions with D_2O. In the reaction of FeO^+ with D_2, three ionic products (Fe^+, FeD^+, and $FeOD^+$) are observed. An inefficient exothermic process that forms $Fe^+ + D_2O$ is observed; however, formation of these products also occurs via another more efficient pathway that involves a reaction barrier of 0.6 eV. It is important to point out that they are able to show that FeO^+ and $Fe^+(a^4F)$ have comparable reactivities that greatly exceed that for $Fe^+(a^6D)$.

Recently a comparison of Fourier transform ion cyclotron resonance (ICR), guided ion beam (GIB), and selected-ion flow tube (SIFT) mass spectrometry methods in the study of gas-phase ion−molecule reactions has been carried out. The purpose was to interpret the experimental findings that agree well in the qualitative description of the low efficiencies of the reaction of $FeO^+ + H_2$, but disagree in the quantitative description of rate constants and branching ratios.[10]

In collaborative work of groups in Berlin and Jerusalem,[11] DFT augmented with CASPT2D computations was used to explore the reaction surface of $FeO^+ + H_2$ and to unravel the origin of the extremely low reactivity observed for this system. According to these calculations, the reaction violates spin-conservation rules and involves a curve crossing from the sextet ground state to the excited quartet surface, giving rise to a multicentered, energetically low-lying transition structure, from which the hydrido iron hydroxide cation $H-Fe-OH^+$ is formed as the initial oxidation product.

Shaik and co-workers[12] continued their studies of the oxidative activation of H−H by FeO^+ using spin−orbit coupling (SOC) calculations. They found that the process involves two spin inversion (SI) junctions between the sextet and quartet states: near the FeO^+/H_2 complex at the entrance channel, and near the Fe^+/H_2O complex at the exit channel. This reduces the probability of the oxidation process even though the quartet surface provides a low-energy path. These groups continued studing this oxidation mechanism[13] with three different DFT functionals: B3LYP, BP86, and FT97. Three mechanisms were considered, addition−elimination, rebound, and oxene insertion.

In the past few years great effort has been made to understand the reaction of MO^+ with hydrogen to yield M^+ and water as products. We have reported here a summary of the works that have focused on the middle transition metal oxide cation reactivy in general, and especially the FeO^+ paradigm. We feel that the debate is still open, and that more data and new perspectives are required. That is, the problem should be examined from another angle, and high-level calculations should be used to describe as accurately as possible the systems of interest that might serve as models for other more complicated organic substrates.[1] Hence, we present here a study of the three middle first-row transition metals in high- and low-spin states in hopes that through the examination of their similarities and differences (and those with the early first-row transition metals) a more complete understanding of their reactivities may be attained.

We present the full reaction mechanism geometries and energetics for both the high- and low-spin states, considering the various possible transition states, intermediates, and products.

2. Methods

The experience of this group[3,4,14] shows that density functional theory (B3LYP functional)[15,16] with the DZVP basis sets given by Salahub et al.[17,18] is a reasonable choice for optimization and frequency calculations of these systems. Recent calibration calculations on transition-metal compounds affirms this choice.[19] The choice of the B3LYP functional is largely motivated by its satisfactory performance reported recently[13,19−25] for transition-metal-containing systems. Reactants and products of the possible reactions have also been reoptimized at the B3LYP/TZVP+G-(3df,2p) level of theory. All the calculations have been corrected with the ZPVE calculated at the corresponding to theoretical level.

To confirm the B3LYP results, some single-point CCSD(T)/TZVP+G(3df,2p) calculations have been carried out at the B3LYP/TZVP+G(3df,2p) equilibrium geometries. The 1s electrons of O and 1s to 2p electrons of the metals were frozen in the CCSD(T) calculations. For the sake of brevity, on occasion in this paper we abbreviate CCSD(T)/TZVP+G(3df,2p)//B3LYP/TZVP+G(3df,2p) as CCSD(T)//B3LYP.

The triple-ζ quality basis set, TZVP+G(3df,2p), used for the metals was that given by Schäfer, Hubert, and Ahlrichs,[26] supplemented with a diffuse s function (with an exponent 0.33 times that of the most diffuse s function on the original set), two sets of p functions optimized by Wachters[27] for the excited states, one set of diffuse pure angular momentum d functions (optimized by Hay),[28] and three sets of uncontracted pure angular momentum f functions, including both tight and diffuse exponents, as recommended by Ragavachari and Trucks.[29] For the oxygen and hydrogen atoms the 6-311++G(2df,2p) basis set of Pople et al.[30] was used.

All DFT and CCSD(T) calculations reported in this paper have been carried out with the GAUSSIAN94/DFT[31] suites of programs. Also NBO[32,33] calculations have been done to give additional insight into the bonding properties of some of the structures.

(10) Schröder, D.; Schwarz, H.; Clemmer, D. E.; Chen, Y.-M.; Armentrout, P. B.; Baranov, V. I.; Bhme, D. K. *Int. J. Mass. Specrom. Ion Processes* **1997**, *161*, 175.
(11) Fiedler, A.; Schröder, D.; Shaik, S.; Schwarz, H. *J. Am. Chem. Soc.* **1994**, *116*, 10734.
(12) Danovich, D.; Shaik, S. *J. Am. Chem. Soc.* **1997**, *119*, 1773.
(13) Filatov, M.; Shaik, S. *J. Phys. Chem. A* **1998**, *102*, 3835.
(14) Irigoras, A.; Ugalde, J. M.; Lopez, X.; Sarasola, C. *Can. J. Chem.* **1996**, *74*, 1824−1829.
(15) Becke, A. D.; *Phys. Rev. A* **1988**, *38*, 3098.
(16) Lee, C.; Yang, W.; Parr, R. G. *Phys. Rev. B* **1988**, *37*, 785.
(17) Sim, F.; Salahub, D. R.; Chim, S.; Dipuis, M. *J. Chem. Phys.* **1991**, *95*, 4317.
(18) Godbout, N.; Salahub, D. R.: Andzelm, J.; Wimmer, E. *Can. J. Chem.* **1992**, *70*, 560.
(19) Bauschlicher, C. W., Jr.; Ricca, A.; Partridge, H.; Langhoff, S. R. In *Recent Advances in Density Functional Theory*; Chong, D. P., Ed.; World Scientific Publishing Co.: Singapore, 1997; Part II.
(20) Sodupe, M.; Branchadell, V.; Rosi, M.; Bauschlicher, C. W., Jr. *J. Phys. Chem. A* **1997**, *101*, 7854−7859.
(21) Siegbahn, P. E. M. Electronic structure calculations for molecules containing transition metals. *Adv. Chem. Phys*. **1996**, *XCIII*.
(22) Ricca, A.; Bauschlicher, C. W. *J. Phys. Chem.* **1994**, *98*, 12899.
(23) Bauschlicher, C. W.; Maitre, P. *J. Phys. Chem.* **1995**, *99*, 3444.
(24) Hartmann, M.; Clark, T.; van Eldik, R. *J. Am. Chem. Soc.* **1997**, *119*, 7843.
(25) Pavlov, M.; Siegbahn, P. E. M.; Sandstrm, M. *J. Phys. Chem. A* **1998**, *102*, 219.
(26) Schäfer, A.; Hurbert, C.; and Ahlrichs, R. *J. Chem. Phys.* **1994**, *100*, 5829.
(27) Wachters, A. J. *J. Chem. Phys.* **1970**, *52*, 1033.
(28) Hay, P. J. *J. Chem. Phys.* **1971**, *66*, 4377.
(29) Raghavachari, K.; Trucks, G. W. *J. Chem. Phys.* **1989**, *91*, 1062.
(30) Krishnan, J. S.; Binkley, J. S.; Seeger, P.v. R.; Pople, J. A. *J. Chem. Phys.* **1980**, *72*, 650.
(31) Frish, M. J.; Trucks, G. W.; Schlegel, H. B.; Gill, P. M. W.; Johnson, B. G.; Robb, M. A.; Cheeseman, J. R.; Keith, T. A.; Petersson, G. A.; Montgomery, J. A.; Raghavachari, K.; Al-Laham, M. A.; Zakrzewski, V. G.; Ortiz, J. V.; Foresman, J. B.; Croslowski, J.; Stefanov, B. B.; Nanayakkara, A.; Challacombe, M.; Peng, C. Y.; Ayala, P. Y.; Chen, W.; Wong, M. W.; Andres, J. L.; Replogle, E. S.; Gomperts, R.; Martin, R. L.; Fox, D. J.; Binkley, J. S.; Defrees, D. J.; Baker, J.; Stewart, J. P.; Head-Gordon, M.; Gonzalez, C.; Pople, J. A. Gaussian 94 (Revision A.1), Gaussian, Inc., Pittsburgh, PA, 1995.

Table 1. Dissociation Energies (D_0 in eV) for the $M(OH_2)^+$ Ion−Molecule Complexes (M = Cr, Mn, Fe)

M	method	D_0
Cr	B3LYP/DZVP	1.481
	B3LYP/TZVP+G(3df,2p)	1.408
	CCSD(T)//B3LYP	1.230
	exptl[39,b]	1.34 ± 0.09
	exptl[40,a]	1.259 ± 0.13
	exptl[41,a]	0.950 ± 0.174
	theory[34] MCPF/[8s6p4d1f]	1.306
	theory[37] QCISD(T)/[8s6p4d1f]	1.390
	theory[37] CCSD(T)(FULL)/6-311++G(d,p)[c]	1.328
Mn	B3LYP/DZVP	1.258
	B3LYP/TZVP+G(3df,2p)	1.196
	CCSD(T)//B3LYP	1.134
	exptl[39,b]	1.23 ± 0.06
	exptl[40,a]	1.411 ± 0.13
	exptl[41,a]	1.150 ± 0.174
	theory[34] MCPF/[86sp4d1f]	1.237
	theory[37] QCISD(T)/[8s6p4d1f]	1.425
	theory[38] CCSD(T)(FULL)/6-311++D(d,p)[c]	1.202
Fe	B3LYP/DZCP	1.469
	B3LYP/TZVP+G(3df,2p)	1.410
	CCSD(T)//B3LYP	1.328
	exptl[39,b]	1.33 ± 0.05
	exptl[40,a]	1.250 ± 0.13
	exptl[41,a]	1.424 ± 0.174
	theory[13] B3LYP/[8s6p4d]	1.515
	theory[13] FT97/[8s6p4d]	1.332
	theory[13] BP86/[8s6p4d1f]	2.174
	theory[34] MCPF/[8s6p4d1f]	1.463
	theory[35] B3LYP/[8s6p4d1f]	1.441
	theory[37] QCISD(T)/[8s6p4d1f]	1.393
	theory[38] CCSD(T)(FULL)/6-31++G(d,p)[c]	1.406

[a] Temperature not specified. [b] Values at 0 K. [c] Values at 298 K.

3. Results and Discussion

3.1. Dissociation Energies. Dissociation energies of the $Cr(OH_2)^+$, $Mn(OH_2)^+$, and $Fe(OH_2)^+$ ion−molecules calculated at the B3LYP/DZVP, B3LYP/TZVP+G(3df,2p), and CCSD(T)//B3LYP levels of theory are shown in Table 1. Dissociation energies were calculated as the difference between the energy of the isolated monomers and the complex, including both BSSE and ZPVE corrections.

$M(OH_2)^+$ dissociation energies predicted by various levels of theory (MCPF/[8s6p4d1f] and B3LYP/[8s6p4d1f] results from Rosi and Bauschlicher,[34−36] QCISD(T) results from Magnusson and Moriarty,[37] and the recent CCSD(T)(FULL)/6-311++G**//MP2(FULL)/6-311++G** results from Trachtman et al.[38]) and those experimentally observed[39−41] are also given in Table 1. For the $Fe(OH_2)^+$ ion−molecule the more recent DFT results from Filatov and Shaik[13] are also listed in Table 1. Note that the temperature is not specified in refs 40 and 41.

Good values are obtained with both the B3LYP and CCSD(T) methods when used in conjunction with the TZVP+G(3df,2p) basis set, as expected from our experience with the early transition-metal calculations.[3,4,14] The difference found between the B3LYP/DZVP and B3LYP/TZVP+G(3df,2p) results is around 0.065 eV, and both are in reasonable agreement with the experimental and theoretical values that can be found in Table 1, especially with the more recent and precise data from Armentrout's group.[39] The CCSD(T) values are systematically lower as is usual for dissociation energies. They are in good agreement with the 1.397 eV CCSD(T)/[8s6p4d1f] D_e value given by Ricca and Bauschlicher.[35] It has been pointed out in our previous work[3,4] that the use of the TZVP+G(3df,2p) basis set with the CCSD(T) method is essential to yield reliable results, for CCSD(T)/DZVP dissociation energies (not shown) are consistently found to be unrealistically low.

Table 2. Relative Energies (eV) for the $^4D(sd^4)$ State of Cr^+ with Respect to the $^6S(d^5)$ Ground State (Δ_1), the $^4A_1$ State of $Cr(OH_2)^+$ with Respect to the $^6A_1$ Ground State (Δ_2), and the $^6\Pi$ State of CrO^+ with Respect to the $^4\Pi$ Ground State (Δ_3)

method	Δ_1	Δ_2	Δ_3
B3LYP/DZVP	2.303	1.532	1.321
B3LYP/TZVP+G(3df,2p)	2.263	1.437	0.136
CCSD(T)//B3LYP	2.257	1.350	0.080
exptl[43]	2.46		

Table 3. Relative Energies (eV) for the $^5S(sd^5)$ State of Mn^+ with Respect to the $^7S(sd^5)$ Ground State (Δ_1), the $^5A_1$ State of $Mn(OH_2)^+$ with Respect to the $^7A_1$ Ground State (Δ_2), and the $^7\Pi$ State of MnO^+ with Respect to the $^5\Pi$ Ground State (Δ_3)

method	Δ_1	Δ_2	Δ_3
B3LYP/DZVP	0.656	0.185	0.464
B3LYP/TZVP+G(3df,2p)	0.856	0.399	0.484
CCSD(T)//B3LYP	0.815	0.677	0.398
exptl[43]	1.17		
theory[1]			0.5
theory[7] CAPT2D/[8s7p6d4f2g]	1.302		0.885
theory[34] MCPF/[8s6p4d1f]		1.866	

Table 4. Relative Energies (eV) for the $^4F(d^7)$ State of Fe^+ with Respect to the $^6D(sd^6)$ Ground State (Δ_1), the $^4B_2$ State of $Fe(OH_2)^+$ with Respect to the $^6A_1$ Ground State (Δ_2), and the $^4\Phi$ State of FeO^+ with Respect to the $^6\Sigma$ Ground State (Δ_3)

method	Δ_1	Δ_2	Δ_3
B3LYP/DZVP	−0.454	−0.701	0.260
B3LYP/TZVP+G(3df,2p)	−0.183	−0.377	0.319
CCSD(T)//B3LYP	0.234	0.119	0.540
exptl[43]	0.25		
theory[11] DFT(NLSD)			1.1
theory[11] CASPT2			0.8
theory[13] B3LYP/[8s6p4d]	−0.104	−0.234	0.347
theory[13] BP86/[8s6p4d]	−0.187	−0.356	0.551
theory[13] FT97/[8s6p4d]	−0.282	−0.486	0.673
theory[34] MCPF/[8s6p4d1f]	0.408	0.191[a]	
theory[35] B3LYP/[8s6p4d1f]	−0.165	0.382[a]	
theory[35] MCPF/[8s6p4d1f]	0.451		
theory[35] CCSD(%)/[8s6p4d1f]	0.360		

[a] Relative energies for their $^6A_1$ and quartet ground state $^4A_1$.

3.2. Excitation Energy. For the reactions of interest there are three high/low-spin relative energies that deserve particular attention. These three are the relative energies between the high- and low-spin states of M^+, $M(OH_2)^+$, and MO^+ species. Excitation energies for these systems are shown in Tables 2 (M = Cr), 3 (M = Mn), and 4 (M = Fe).

The high/low-spin splittings for these three metal ions follow the trends observed for the early transition-metal ions. That is, our values are always lower than the experimental ones, and the best overall fitting is obtained at the CCSD(T)//B3LYP level of theory. Cr^+ and Mn^+ excitation energies are predicted

(32) Read, A. E.; Curtiss, L. A.; Weinhold, F. *Chem. Rev.* **1988**, *88*, 899.
(33) NBO Version 3.1: Glendening, A. E.; Read, A. E.; Carpenter, J. E.; Weinhold, F.
(34) Rosi, M.; Bauschlicher, C. W. *J. Chem. Phys.* **1989**, *90* (12), 7264; **1990**, *92* (3), 1876.
(35) Ricca, A.; Bauschlicher, C. W. *Theor. Chim. Acta* **1995**, *92*, 123.
(36) Ricca, A.; Bauschlicher, C. W. *J. Phys. Chem.* **1995**, *99*, 9003.
(37) Magnusson, E.; Moriarty, N. W. *J. Comput. Chem.* **1993**, *14* (8), 961.
(38) Trachtman, M.; Markham, G. D.; Glusker, J. P.; George, P.; Bock, C. W. *Inorg. Chem.* **1998**, *37*, 4421.
(39) Dalleska, N. F.; Honma, K.; Sunderlin, L. S. Armentrout, P. B. *J. Am. Chem. Soc.* **1994**, *116*, 3519.
(40) Magnera, T. F.; David, D. E.; Michl, J. *J. Am. Chem. Soc.* **1989**, *111*, 4100.
(41) Marinelli, P. J.; Squires, R. R. *J. Am. Chem. Soc.* **1989**, *111*, 4101.

Table 5. Relative Energies (eV) for the Different States of $Fe(OH_2)^+$

state	B3LYP/DZVP	B3LYP/TZVP+G(3df,2p)	CCSD(T)//B3LYP
$^6A_1$	0.000	0.000	0.000
$^6A_2$	−0.005	−0.005	0.002
$^6B_2$	0.104	0.095	0.100
$^4B_2$	−0.701	−0.377	0.119
$^4A_2$	−0.716	−0.379	0.176
$^4A_1$	−0.710	−0.375	0.177
$^6B_1$	0.202	0.196	0.187
$^4B_1$	−0.606	−0.294	0.196

satisfactorily by the B3LYP and CCSD(T) methods; indeed it is the B3LYP method which holds a slight advantage in average error for the two species. However, in the case of the $^6D(sd^6) \rightarrow {}^4F(d^7)$ splitting of Fe^+, the B3LYP method is far from the mark, even incorrectly predicting the ordering of the states. This is a known problem that has been extensively discussed in the literature,[13,35,36,42] and that has been attributed to a bias toward $3d^n$ configurations over $3d^{n-1}4s^1$, which is inherent in density functionals, regardless of whether they are pure or hybrid. We have taken the ^6D state of the iron ion as the energy of reference for all the calculations throughout this work, even at the B3LYP levels of theory. Notice that with the CCSD(T) method the ordering of the states is correct and the relative gaps are well described. The value obtained is in very good agreement with the experimental result of Moore,[43] and it is in better agreement than is the value calculated by Bauschlicher and co-workers at the MCPF level.

High-spin → low-spin excitation energies for the $M(OH_2)^+$ ion−molecules also have been calculated. Here the $Cr(OH_2)^+$ ion−molecule mantains the trend observed for the early transition metals, that is, CCSD(T) values give smaller splittings than B3LYP, but this is not the case for the $Mn(OH_2)^+$ ion−molecule, where we obtain a higher gap at the CCSD(T) level of theory, but much smaller than the one calculated by Rosi and Bauschlicher.[34] For the $Fe(OH_2)^+$ ion−molecule, again, we cannot properly describe the ordering of the states with the B3LYP method, as the relative stability of the $Fe(OH_2)^+$ system is dependent upon the $^6D(sd^6) \rightarrow {}^4F(d^7)$ splitting in Fe^+. At the B3LYP level of theory the $^4A_2$ state is the most stable. In Table 5 we have listed several states calculated at the B3LYP/DZVP, B3LYP/TZVP+G(3df,2p), and CCSD(T)//B3LYP levels of theory. Ab initio MCPF results from Rosi and Bauschlicher[34] predict a quartet state $^4A_1$ 0.191 eV above the $^6A_1$ sextet ground state. That value is in good accordance with our CCSD(T)//B3LYP value. From Table 5 it can be seen that the relative energies among the various sextets are quite consistent across the table. It is in describing the low-spin → high-spin splitting that the B3LYP method gives results which contrast so sharply with those of the CCSD(T) method.

The last species studied at these levels was the metal oxide cation MO^+ molecule. For Cr and Mn^+ the low-spin moieties are still the ground states, but for Fe the high-spin moiety is the ground state. This is because the CrO^+ and MnO^+ molecules have no paired electrons in a M−O σ bond, while the sextet Fe−O^+ molecule, with one electron more than MnO^+, places that electron in the M−O σ bond. Now the tendencies are correctly described at all theoretical levels used. Smaller gaps are obtained at the CCSD(T)//B3LYP level of theory, and in general they agree with the other theoretical values found in the literature; the range of predicted values is, however, quite large.

3.3. Reaction Energetics. 3.3.1. $Cr^+(^6S) + H_2O$. Equations 1−8 represent the main ionic products observed in the reaction of $Cr^+(^6S)$ with H_2O. The predicted ΔE energies are listed in Table 6 together with the estimation of Kang and Beauchamp[6] for reaction 1, and the values for several other reactions extracted from the available thermodynamical data.[44]

$$Cr^+(^6S) + H_2O \rightarrow CrO^+(^4\Pi) + H_2 + \Delta E_1 \quad (1)$$

$$Cr^+(^6S) + H_2O \rightarrow CrO^+(^6\Pi) + H_2 + \Delta E_2 \quad (2)$$

$$Cr^+(^6S) + H_2O \rightarrow HCrO^+(^3A'') + H + \Delta E_3 \quad (3)$$

$$Cr^+(^6S) + H_2O \rightarrow HCrO^+(^5A') + H + \Delta E_4 \quad (4)$$

$$Cr^+(^6S) + H_2O \rightarrow CrOH^+(^3A') + H + \Delta E_5 \quad (5)$$

$$Cr^+(^6S) + H_2O \rightarrow CrOH^+(^5A') + H + \Delta E_6 \quad (6)$$

$$Cr^+(^6S) + H_2O \rightarrow CrH^+(^3\Sigma) + OH + \Delta E_7 \quad (7)$$

$$Cr^+(^6S) + H_2O \rightarrow CrH^+(^5\Sigma) + OH + \Delta E_8 \quad (8)$$

3.3.2. $Mn^+(^7S) + H_2O$. Equations 9−16 represent the main ionic products of the reaction of $Mn^+(^7S)$ and H_2O. Table 7 lists the calculated ΔE values along with the three experimental measurements of Ryan and co-workers,[7] and the values for several other reactions extracted from the available thermodynamical data.[44]

$$Mn^+(^7S) + H_2O \rightarrow MnO^+(^5\Pi) + H_2 + \Delta E_9 \quad (9)$$

$$Mn^+(^7S) + H_2O \rightarrow MnO^+(^7\Pi) + H_2 + \Delta E_{10} \quad (10)$$

$$Mn^+(^7S) + H_2O \rightarrow HMnO^+(^4A'') + H + \Delta E_{11} \quad (11)$$

$$Mn^+(^7S) + H_2O \rightarrow HMnO^+(^6A'') + H + \Delta E_{12} \quad (12)$$

$$Mn^+(^7S) + H_2O \rightarrow MnOH^+(^4A') + H + \Delta E_{13} \quad (13)$$

$$Mn^+(^7S) + H_2O \rightarrow MnOH^+(^6A') + H + \Delta E_{14} \quad (14)$$

$$Mn^+(^7S) + H_2O \rightarrow MnH^+(^4\Sigma) + OH + \Delta E_{15} \quad (15)$$

$$Mn^+(^7S) + H_2O \rightarrow MnH^+(^6\Sigma) + OH + \Delta E_{16} \quad (16)$$

3.3.3. $Fe^+(^6D) + H_2O$. The corresponding equations for the main ionic products resulting in the reaction of $Fe^+(^6D)$ with H_2O are shown below. The various predicted ΔE values and the values extracted from the available thermodynamical data,[44]

(42) Holthausen, M. C.; Fiedler, A.; Schwarz, H.; Koch, W. *J. Phys. Chem.* **1996**, *100*, 6236.

(43) Moore, C. E. *Atomic Energy Levels*; National Bureau of Standards: Washington, DC, 1952; Natural Bureau of Standards Circular, 1959; pp 2, 3, 467.

(44) (a) Chase, M. W.; Davies, C. A.; Downey, J. R.; Frurip, D. J.; McDonald, R. A.; Syvened, A. N. *J. Phys. Chem. Ref. Data* **1985**, *14*, Suppl. No. 1 (JANAF tables). (b) Gurvich, L. V.; Veyts, I. V.; Alcock, C. B. *Thermodynamic Properties of Individual Substances*, 4th ed.; Hemisphere: New York, 1989; Vol. 1, Part 2. (c) Armentrout, P. B. In *Gas-Phase Inorganic Chemistry*; Russell, D. H., Ed.; Plenum Press: New York, 1989; p 1. (d) Armentrout, P. B.; Kickel, B. L. In *Organometallic Ion Chemistry*; Freiser B. S., Ed.; Kluwer: Dordrecht, The Netherlands, 1996; p 1.

Table 6. Overall Energies for Reactions 1−8 at Several Levels of Theory[a]

method	ΔE_1	ΔE_2	ΔE_3	ΔE_4	ΔE_5	ΔE_6	ΔE_7	ΔE_8
B3LYP/DZVP	−1.912	−3.233	−4.755	−6.202	−3.528	−2.239	−5.048	−3.461
B3LYP/TZVP+G(3df,2p)	−1.754	−1.890	−4.431	−5.945	−3.332	−2.073	−4.983	−3.430
CCSD(T)//B3LYP	−1.962	−2.042	−4.730	−6.068	−3.471	−2.321	−4.956	−3.783
exptl[6,11]	−1.389							
exptl[44]	−1.31± 0.12					−2.03± 0.15		−3.75± 0.09

[a] Energies given are in electronvolts and for the various B3LYP levels of theory include ZPVE corrections calculated at the corresponding level of theory.

Table 7. Overall Energies for Reactions 9−16 at Several Levels of Theory[a]

method	ΔE_9	ΔE_{10}	ΔE_{11}	ΔE_{12}	ΔE_{13}	ΔE_{14}	ΔE_{15}	ΔE_{16}
B3LYP/DZVP	−2.006	−2.470	−5.115	−6.249	−3.378	−1.501	−4.181	−2.655
B3LYP/TZVP+G(3df,2p)	−2.164	−2.648	−5.178	−6.304	−3.631	−1.634	−4.447	−2.841
CCSD(T)//B3LYP	−2.638	−3.036	−5.884	−6.701	−4.519	−1.940	−4.525	−3.184
exptl[44]	−2.08 ± 0.13					−1.68 ± 0.25		−3.06 ± 0.15
theory[7] CAPT2D/[8s7p6d4f2g]	−2.17	−3.125				−1.736		

[a] Energies given are in electronvolts and for the various B3LYP levels of theory include ZPVE corrections calculated at the corresponding level of theory.

Table 8. Overall Energies for Reactions 17−24 at Several Levels of Theory[a]

method	ΔE_{17}	ΔE_{18}	ΔE_{19}	ΔE_{20}	ΔE_{21}	ΔE_{22}	ΔE_{23}	ΔE_{24}
B3LYP/DZVP	−1.560	−1.300	−4.665	−5.705	−2.172	−0.980	−3.096	−2.210
B3LYP/TZVP+G(3df,2p)	−1.760	−1.441	−4.796	−5.538	−2.379	−1.136	−3.437	−2.459
CCSD(T)//B3LYP	−2.155	−1.615	−5.255	−5.836	−2.652	−1.434	−3.965	−2.831
exptl[44]		−1.56 ± 0.06				−1.32 ± 0.12		−3.00 ± 0.06
theory[11] CASPT2D/[8s7p6d4f2g]		−1.562						
theory[13] B3LYP/[8s6p4d]	−2.018	−1.671				−1.432		
theory[13] BP86/[8s6p4d]	−0.716	−0.165				−0.425		
theory[13] FT97/[8s6p4d]	−1.007	−0.334				−0.933		

[a] Energies given are in electronvolts and for the various B3LYP levels of theory include ZPVE corrections calculated at the corresponding level of theory.

Table 9. Geometrical Parameters of the Various $M(OH_2)^+$ Stationary Points on the B3LYP/DZVP and B3LYP/TZVP+G(3df,2p) Potential Energy Surfaces[a]

		B3LYP/DZVP			B3LYP/TZVP+G(3df,2p)		
metal	state	M−O	O−H	M−O−H	M−O	O−H	M−O−H
Cr	$^4A_1$	2.048	0.972	126.1	2.021	0.966	125.7
Cr	$^6A_1$	2.093	0.971	126.5	2.087	0.965	126.2
Mn	$^5A_1$	2.042	0.973	126.1	2.045	0.967	125.8
Mn	$^7A_1$	2.193	0.974	126.7	2.191	0.968	126.5
Fe	$^4B_2$	2.006	0.971	126.3	2.006	0.965	126.2
Fe	$^6A_1$	2.119	0.975	126.2	2.101	0.969	126.1

[a] Bond lengths are reported in angstroms and bond angles in degrees.

along with the theoretical estimates of Fiedler and co-workers[11] and Filatov,[13] are listed in Table 8.

$$Fe^+(^6D) + H_2O \rightarrow FeO^+(^4\Phi) + H_2 + \Delta E_{17} \quad (17)$$

$$Fe^+(^6D) + H_2O \rightarrow FeO^+(^6\Sigma) + H_2 + \Delta E_{18} \quad (18)$$

$$Fe^+(^6D) + H_2O \rightarrow HFeO^+(^3A') + H + \Delta E_{19} \quad (19)$$

$$Fe^+(^6D) + H_2O \rightarrow HFeO^+(^5A'') + H + \Delta E_{20} \quad (20)$$

$$Fe^+(^6D) + H_2O \rightarrow FeOH^+(^3A'') + H + \Delta E_{21} \quad (21)$$

$$Fe^+(^6D) + H_2O \rightarrow FeOH^+(^5A') + H + \Delta E_{22} \quad (22)$$

$$Fe^+(^6D) + H_2O \rightarrow FeH^+(^3X) + OH + \Delta E_{23} \quad (23)$$

$$Fe^+(^6D) + H_2O \rightarrow FeH^+(^5\Delta) + OH + \Delta E_{24} \quad (24)$$

3.4. Stationary Points. Tables 9−13 show the most relevant stationary points found for the $M(OH_2)^+$, $TS1^+$, HM^+OH, $TS2^+$, and $(H_2)MO^+$ species, respectively, calculated at the B3LYP/DZVP and B3LYP/TZVP+G(3df,2p) (in parentheses) levels of theory, where M = Cr, Mn, and Fe.

In Table 9 are listed the geometrical parameters for the $M(OH_2)^+$ ion−molecule complexes. The C_{2v} symmetry $Cr(OH_2)^+$ ion−molecule complex has a Cr−O distance of 2.048 Å in the quadruplet state and 2.093 Å in the sextet isomer. The ground states at the quadruplet and sextet states are $^4A_1$ and $^6A_1$, respectively. Excited states have been calculated, and all of them lie far from these ground states.

The $Mn(OH_2)^+$ ion−molecule complex has a Mn−O distance of 2.042 Å in the low-spin ($^5A_1$) case and a bond length of 2.193 Å in the high-spin ($^7A_1$) state. Note that there is a large difference between the Mn−O distance of the low-spin and high-spin cases. While this difference is 0.151 Å for Mn, it is 0.047, 0.001, 0.024, and 0.045 Å for Sc, Ti, V, and Cr respectively. The septet Mn^+ ion with its complete half-filling of shells (s^1d^5) is not predisposed to accepting donations from the H_2O molecule for it will reduce its large stabilizing exchange energy. Indeed pairing the spin of two of its electrons causes a substantial

Table 10. Geometrical Parameters of the Various $TS1^+$ Transition States on the B3LYP/DZVP and B3LYP/TZVP+G(3df,2p) (in Parentheses) Potential Energy Surfaces[a]

metal	state	M−O	M−H(1)	O−H(1)	O−H(2)	M−O−H(1)
Cr	4	1.793	1.710	1.325	0.974	64.5
Mn	5	1.806	1.628	1.513	0.974	57.9
Mn	^{7}A′	1.778	2.214	2.128	0.971	68.4
Fe	^{4}A″	1.749 (1.747)	1.557 (1.590)	1.548 (1.624)	0.974 (0.968)	56.0 (56.2)
Fe	^{6}A′	1.795 (1.798)	1.781 (1.741)	1.605 (1.607)	0.980 (0.972)	62.9 (61.2)

[a] Bond lengths are reported in angstroms and bond angles in degrees.

Table 11. Geometrical Parameters of the Various $H(1)M^+OH(2)$ Stationary Points on the B3LYP/DZVP and B3LYP/TZVP+G(3df,2p) (in Parentheses) Potential Energy Surfaces[a]

metal	state	M−H(1)	M−O	O−H(2)	H(1)−M−O	M−O−H(2)
Cr	^{4}A″	1.572	1.708	0.981	97.1	132.3
Cr	^{6}A′	2.230	1.756	0.972	138.7	104.9
Mn	^{5}A′	1.563	1.722	0.977	91.6	130.5
Mn	^{7}A′	2.100	1.759	0.971	192.6	140.8
Fe	^{4}A″	1.509 (1.518)	1.690 (1.687)	0.978 (0.970)	87.2 (90.9)	131.8 (130.5)
Fe	^{6}A′	1.594 (1.587)	1.746 (1.733)	0.979 (0.969)	131.3 (139.6)	141.7 (143.1)

[a] Bond lengths are reported in angstroms and bond angles in degrees.

Table 12. Geometrical Parameters of the Various $TS2^+$ Transition States on the B3LYP/DZVP and B3LYP/TZVP+G(3df,2p) (in parentheses) Potential Energy Surfaces[a]

metal	state	M−H(1)	M−O	O−H(2)	H(1)−H(2)	H(1)−M−O	M−O−H(2)
Cr	^{4}A″	1.732	1.650	1.310	1.011	78.3	72.6
Cr	^{6}A′	2.539	1.815	1.471	0.808	57.7	89.3
Mn	^{5}A′	1.780	1.661	1.443	0.904	78.3	70.5
Fe	^{4}A″	1.667 (1.683)	1.619 (1.614)	1.415 (1.421)	0.933 (0.934)	82.3 (82.1)	68.3 (68.8)
Fe	^{6}A′	1.861 (1.809)	1.751 (1.728)	1.276 (1.310)	1.007 (1.013)	72.6 (76.0)	74.1 (71.5)

[a] Bond lengths are reported in angstroms and bond angles in degrees.

decrease of the Mn−O bond length, at the B3LYP/TZVP+G(3df,2p) level of theory, 0.156 Å for the resulting $^5A_1$ state and 0.165 Å for the resulting $^5B_2$ state, and a concomitant energy destabilization, 0.399 eV for the $^5A_1$ state and 0.880 eV for the $^5B_2$ state.

Things are a bit more involved for the $Fe(OH_2)^+$ ion−molecule complex. As can be seen in Table 5 several states lie very close in energy, and the B3LYP and CCSD(T) results are not in accordance. While the high-spin ground state ($^6A_1$) is the lowest lying of all the states listed in Table 5 at the CCSDT//B3LYP level, it is the $^4A_2$ low-spin state that corresponds to the ground state at either the B3LYP/DZVP or B3LYP/TZVP+G(3df,2p) level. We took the CCSD(T)//B3LYP predictions as the correct ones, and so we show the values for the corresponding $^4B_2$ and $^6A_1$ states. For the $^4B_2$ state the Fe−O bond length is 2.006 eV, and 2.119 eV for the $^6A_1$ state.

As we pointed out in our previous work,[4] as we progress from Sc to V, this M−O distance among these complexes shrinks, the V−O distance being 2.085 and 2.109 Å for the $^3A_1$ and $^5A_1$ states, respectively. The trend holds for the low-spin state, but it breaks at Mn for the high-spin state. However, as we pointed out earlier, this is due to the fact that $Mn(OH_2)^+$-($^7A_1$) has the maximun attainable exchange energy.

$TS1^+$ characterizes the initial hydrogen transfer from oxygen to the metal. Geometrical data corresponding to this transition state can be found in Table 10. This transition state has near-C_s symmetry, and the one imaginary frequency clearly corresponds to the hydrogen migration over the metal atom.

The HM^+OH minimum has C_s symmetry in all cases. This intermediate is a well-characterized minimum for all the reactions. However, as can be seen in Table 11 there is an appreciable difference between the low- and high-spin M−H bond distances for the Cr and Mn moieties in accordance with the previous values reported for the early transition metal ions. The Mn species in the high-spin state is the only one that exhibits a trans conformation. No cis conformer was found despite extensive search. The low-spin cases follow the expected trend, with the M−H bond distance decreasing from Cr to Fe.

A drastic reduction of the M−H bond is also observed for the high-spin cases. The reduction seen in moving from Cr to Mn is not out of the ordinary, but the change from Mn to Fe is remarkable (from 2.10 to 1.59 Å). This is because in the case of ^{7}A′ HMn^+OH there are no paired electrons in the Mn−H interaction. The ^{6}A′ HFe^+OH intermediate, however, has a pair of electrons in the Fe−H σ bond, according to our NBO analysis.

Our geometrical prediction agrees well with earlier results from other groups,[11,13] but we disagree concerning the bonding nature of ^{6}A′ HFe^+OH. They explain that the lengthening in the Fe−H distance from the quartet to the sextet electromers (1.51 Å versus 1.59 Å in Fiedlers' results,[11] and 1.523 Å versus 1.587 Å in Shaiks' results[13]) is due to the different character in the Fe−H bonding. As was the case for all the other metals studied, they assign a weak coordination of H$^\bullet$ to a high-spin $FeOH^+$. However, our NBO results clearly assign a covalent bond in both the low- *and* high-spin cases, and the comparison to HMn^+OH is also supportive of the argument for a covalent bond. The assignment of two electrons to a covalent Fe−H bond, however, leaves us with a lack of paired electrons for Fe−O bonding. The same NBO analysis which gives a pair of electrons to the Fe−H bond reports two singly occupied Fe−O bonds, and a strong donation from an *O* lone pair into the σ^*_{Fe-H} bond.

The second oxygen to metal hydrogen transfer occurs through $TS2^+$ depicted in Table 12. For the low-spin isomers, these transition states show H−H distances which are still quite long for a bond (1.011 Å for Cr, 0.904 Å for Mn, and 0.933 Å for Fe), even though they are slightly shorter than the values found

Table 13. Geometrical Parameters of the Various $(H_2)MO^+$ Stationary Points on the B3LYP/DZVP and B3LYP/TZVP+G(3df,2p) (in parentheses) Potential Energy Surfaces[a]

metal	state	M−O	M−H(1)	M−H(2)	H−H	H−M−O
Cr	$^4A''$	1.588	2.009	1.997	0.767	108.3
Cr	$^6A'$	1.836	2.062	2.062	0.763	90.5
Mn	$^5A'$	1.724	2.124	2.124	0.762	180.0
Mn	$^7A'$	1.848	2.112	2.112	0.762	180.0
Fe	$^4A''$	1.565 (1.558)	1.761 (1.774)	1.761 (1.774)	0.793 (0.796)	96.9 (97.8)
Fe	$^6A'$	1.663 (1.643)	2.002 (1.995)	2.002 (1.995)	0.765 (0.769)	180.0

[a] Bond lengths are reported in angstroms and bond angles in degrees.

for the Sc−V series.[3,4] The one imaginary frequency corresponds to H−H bond formation and O−H bond-breaking.

The high-spin four-centered transition states show an almost fully formed H−H bond and very long M−H and O−H bond distances for Cr. Also, the imaginary frequency is reminiscent of direct H_2 elimination. However, for the corresponding $TS2^+$ in the Fe system this H−H bond is even larger than the corresponding bond in the low-spin transition state, again demonstrating the similarities between the low- and high-spin structures on the $Fe^+ + H_2O$ surface, and again due to the presence of a pair of electrons in the valence shell of Fe^+ even in the high-spin cases—something *all* the earlier high-spin M^+ ions lacked.

The final stationary points located were the $(H_2)MO^+$ hydrogen molecule metal oxide adduct illustrated in Table 13. As was pointed out for the Ti system[3] this minimum should be considered an ion−molecule complex. For all of them the M−H bond distance has increased from the HM^+OH minimum to the corresponding $(H_2)MO^+$ minimum, as was expected, but this increase is much less in the M = Fe case, where there is an increase of only 0.252 Å, while for the M = Cr case the increase is 0.437 Å. Also for these three systems the examination of the MOs shows an interaction between the singly-occupied d orbital of M and the σ^*_{H-H} orbital (see Figure 2 of ref 3). The NBO analysis gives this interaction a value of 3.45 kcal/mol for Cr, 1.96 kcal/mol for Mn, and 5.09 kcal/mol for Fe, smaller than for the Ti (7.87 kcal/mol) and V (5.45 kcal/mol) cases reported previously. It is through this interaction that the H−H bond is activated by the oxide in the reverse reaction. The back-donation from the σ_{H-H} orbital to the metal's s orbital should also be remarked upon. The NBO analysis gives that donation a value of 5.56 kcal/mol in the case of Cr and 11.77 kcal/mol in the case of Fe. No donation was found for the Mn case as the s orbital is the one used in the bonding with oxygen; however, a $\sigma_{H-H} \rightarrow \sigma^*_{Mn-O}$ donation of 6.97 kcal/mol is encountered.

It should be pointed out that we found another $^5A'$ structure for the $(H_2)MnO^+$ species, where the interaction between the singly-occupied d orbital of Mn and the σ^*_{H-H} orbital is 2.36 kcal/mol. This slightly high-lying excited state (0.293 eV at the B3LYP/DZVP level) has a smaller Mn−O distance (1.595 Å) than the ground state (1.724 Å), and has a 5.85 kcal/mol donation from the σ_{H-H} orbital to the metal s orbital, where one of the d orbitals is used in the bonding with oxygen.

3.5. Potential Energy Surfaces. For the Sc^+-Mn^+ reactions the principal product of the $M^+ + H_2O$ reaction was the low-spin metal oxide ion, but this in not the case for the Fe^+ reaction, where the $^6\Sigma$ high-spin state is the ground state FeO^+. This is the reason for discussing the PESs in two subsections. Also, the iron system is particularly difficult to describe at the B3LYP level of theory since the correct ordering for the spin states of the Fe^+ cation is not obtained as pointed out earlier.[13,35,36,42] Thus, results obtained with higher levels of theory will also be discussed.

That the different spin structures are located in the same column should not be taken to mean that they are connected by simple vertical excitation. The geometrical parameters are significantly different as can be seen in Tables 9−13.

3.5.1. Chromium and Manganese Cases. Figures 1 and 2 show the potential energy surface starting from the $M^+ + OH_2$ separated reactants and leading to the products $MO^+ + H_2$ for the low- and high-spin states at the B3LYP/DZVP level of theory for Cr^+ and Mn^+, respectively.

The surfaces for the reactions of both Cr^+ and Mn^+ are similar to those we have reported earlier,[3,4] with the first step being the formation of the $M(OH_2)^+$ ion−molecule complex. Through $TS1^+$, one hydrogen atom is passed from oxygen to the metal, leading to the HM^+OH molecule, the intermediate whose existence was surmised by experimentalists. As was observed for V^+, but not for Sc^+ or Ti^+, on the low-spin surface the $TS1^+$ transition state lies above the energy of the high-spin ground-state reactants.

The second hydrogen transfer from oxygen to the metal takes place through $TS2^+$. This transition state leads to the final intermediate found on the reaction path: the $(H_2)MO^+$ ion−molecule complex. In the case of M = Cr, this complex is bound by 0.455 eV, while it is bound by 0.407 eV in the case of Mn. These values are larger than the ones observed for Sc (0.270 eV), Ti (0.375 eV), and V (0.353 eV). From this intermediate the loss of H_2 proceeds without a transition state to the low-spin MO^+ and H_2.

The first step on the high-spin surface can also be formation of the ion−molecule complex. Note, however, that the high-spin $Mn(OH_2)^+$ complex is not as stabilized as were the other species due to the complete half-filled valence shell of ^7S Mn^+. Despite numerous varied strategies for finding a transition state between this complex and the HCr^+OH molecule, none was found, as was the case for the Sc triplet and Ti quartet surfaces. This was not the case for the quintet surface for V^+ and septuplet surface for Mn^+. A septuplet $TS1^+$ has been found on the $Mn^+ + H_2O$ surface corresponding to the migration of one hydrogen from oxygen to manganese. The high-spin → low-spin splitting for this transition state is much greater than it was in the case of the V^+ system (0.928 eV for Mn^+ vs 0.143 eV for V^+).

Once the high-spin HM^+OH intermediate is formed, another intermediate, $(H_2)MO^+$, can be realized by passing through another high-lying H transfer transition state, $TS2^+$. This $TS2^+$ in the Cr^+ case lies 0.997 eV higher in energy than the corresponding low-spin transition state. From that isomer, the loss of an H_2 molecule gives one of the reaction products, high-spin MO^+. No high-spin $TS2^+$ isomer has been encountered for the Mn^+ system.

These reaction pathways follow the same general scheme as was seen for the early first-row transition metals, with the low- and high-spin surfaces crossing between the $M(OH_2)^+$ and HM^+-OH structures. There are many specific differences between the potential energy surfaces of the $M^+ + H_2O$ (M = Sc−Mn) series, but the same pathway to products $MO^+ + H_2$ is followed, and there is a definite trend of increasing barrier heights and endothermicity as we move from left to right along the periodic table.

Equilibrium geometry parameters for the various reaction products are given in Table 14.

3.5.2. Iron Case. Figure 3 shows the potential energy surface starting from the $Fe^+ + OH_2$ separated reactants and leading to

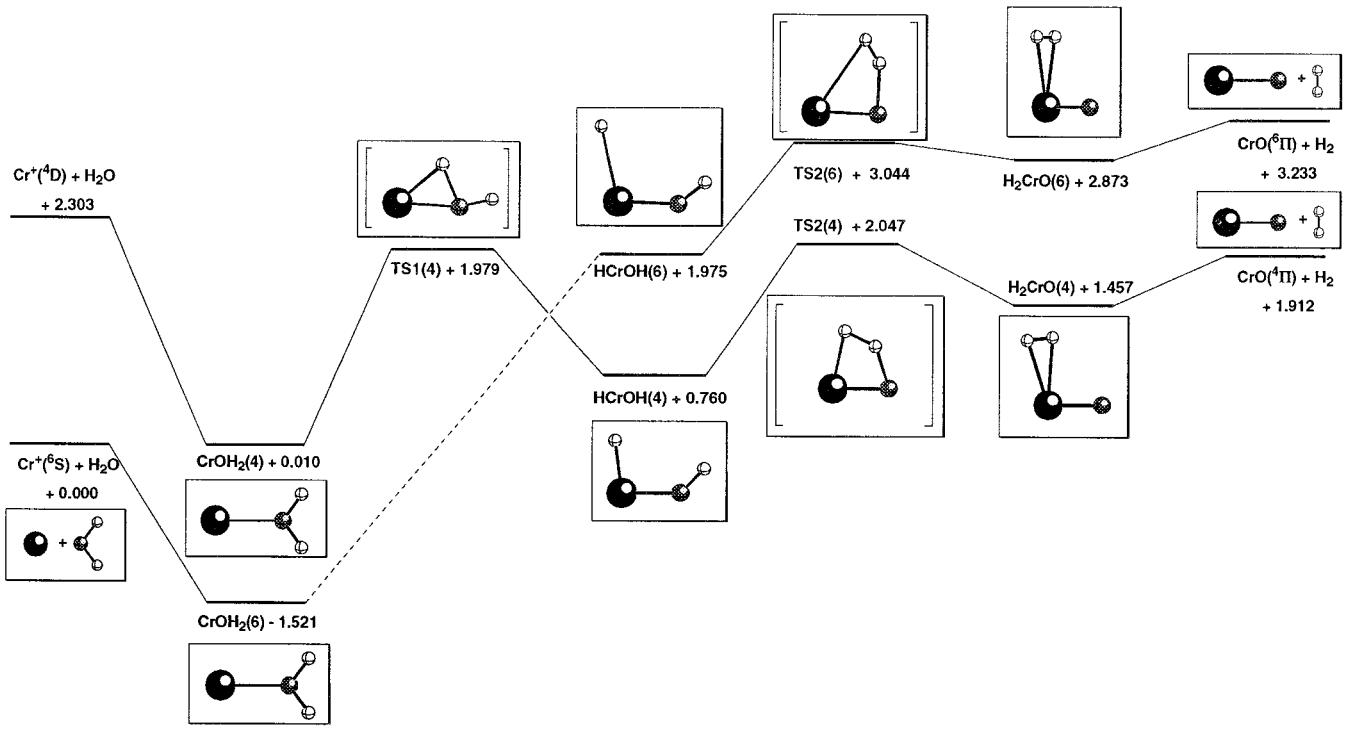

Figure 1. B3LYP/DZVP potential energy surface following the $Cr^+ + OH_2 \rightarrow CrO^+ + H_2$ reaction path. Energies given are in electronvolts and are relative to the separated ground-state reactants, $Cr^+(^6S) + OH_2$.

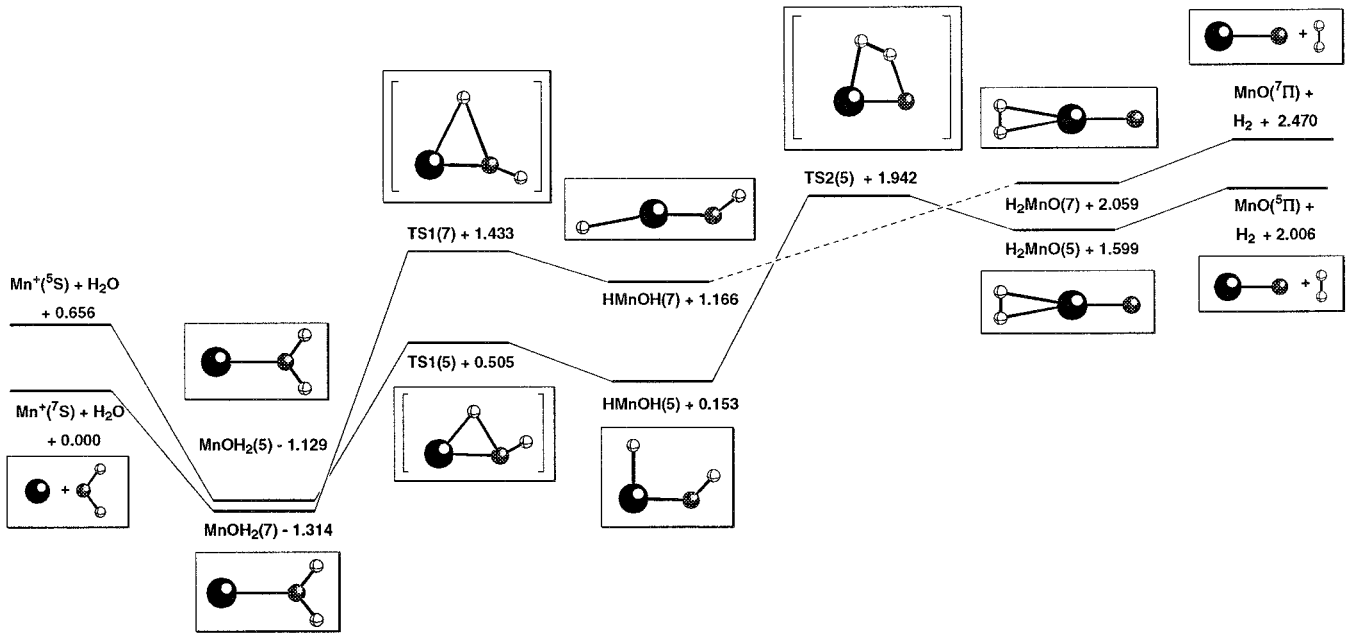

Figure 2. B3LYP/DZVP potential energy surface following the $Mn^+ + OH_2 \rightarrow MnO^+ + H_2$ reaction path. Energies given are in electronvolts and are relative to the separated ground-state reactants, $Mn^+(^7S) + OH_2$.

the products $FeO^+ + H_2$ for the low- and high-spin states at the CCSD(T)//B3LYP level of theory. Due to the misleading description at the B3LYP level of theory, no potential energy surface is shown for this system at that level of theory.

The potential energy surface for the $Fe^+ + H_2O$ system is fairly complicated. Danovich and Shaik[12] predicted two spin crossings for this reaction—one between $Fe(OH_2)^+$ and HFe^+-OH and a second between HFe^+OH and H_2FeO^+. The first step is the formation of the $Fe(OH_2)^+$ ion−molecule complex. Through $TS1^+$, one hydrogen atom is passed from oxygen to the metal, leading to the HFe^+OH intermediate. In all results reported in the literature and in our own results this sextuplet transition state lies higher in energy than the quartet one. However, this accordance is not obtained for the HFe^+OH intermediate. All DFT results agree in assigning a quartet ground state, but as larger basis sets are used the splitting between the two states becomes smaller. At the B3LYP/DZVP level of theory a 0.493 eV value is obtained, and at the B3LYP/TZVP+G(3df,2p) level the value is reduced to 0.194 eV. The group in Berlin gives a 0.477 eV splitting value calculated at the CASPT2 level, and the group in Jerusalem[13] reports a 0.130 eV value with the B3LYP functional, 0.325 eV with BP86, and 0.351 eV with FT97. All these results seem to agree quite well, but the surprise comes with our CCSD(T)//B3LYP results, where

Table 14. Equilibrium Geometry Parameters for the Various $M^+ + OH_2$ Reaction Products at the B3LYP/DZVP and B3LYP/TZVP+G(3df,2p) Levels of Theory[a]

			B3LYP/DZVP			B3LYP/TZVP+G(3df,2p)		
product	metal	state	M−O	M−H	angle	M−O	M−H	angle
MO^+	Cr	$^4\Pi$	1.586			1.572		
		$^6\Pi$	1.831			1.829		
	Mn	$^5\Pi$	1.723			1.729		
		$^7\Pi$	1.850			1.852		
	Fe	$^4\Phi$	1.689			1.696		
		$^6\Sigma$	1.655			1.637		
MH^+	Cr	$^3\Sigma$		1.580		1.586		
		$^5\Sigma$		1.598		1.602		
	Mn	$^4\Sigma$		1.578		1.574		
		$^6\Sigma$		1.587		1.612		
	Fe	$^3\Phi$		1.529		1.532		
		$^5\Delta$		1.559		1.574		
HMO^+	Cr	$^3A''$	1.537	1.575	100.3	1.520	1.585	106.6
		$^5A'$	1.583	2.301	117.2	1.568	2.242	132.9
	Mn	$^4A''$	1.662	1.555	91.7	1.654	1.566	95.6
		$^6A''$	1.726	2.188	179.9	1.731	2.142	179.7
	Fe	$^3A'$	1.634	1.504	88.8	1.630	1.512	91.6
		$^5A''$	1.728	1.649	120.8	1.736	1.610	125.1
MOH^+	Cr	$^3A'$	1.737	0.973	140.0	1.737	0.965	138.3
		$^5A'$	1.753	0.973	137.0	1.751	0.965	135.8
	Mn	$^4A'$	1.722	0.975	140.7	1.715	0.967	137.8
		$^6A'$	1.744	0.970	146.1	1.751	0.963	140.5
	Fe	$^3A''$	1.725	0.975	139.1	1.718	0.968	133.9
		$^5A'$	1.712	0.972	144.2	1.715	0.965	140.1

[a] Bond lengths are reported in angstroms and bond angles in degrees.

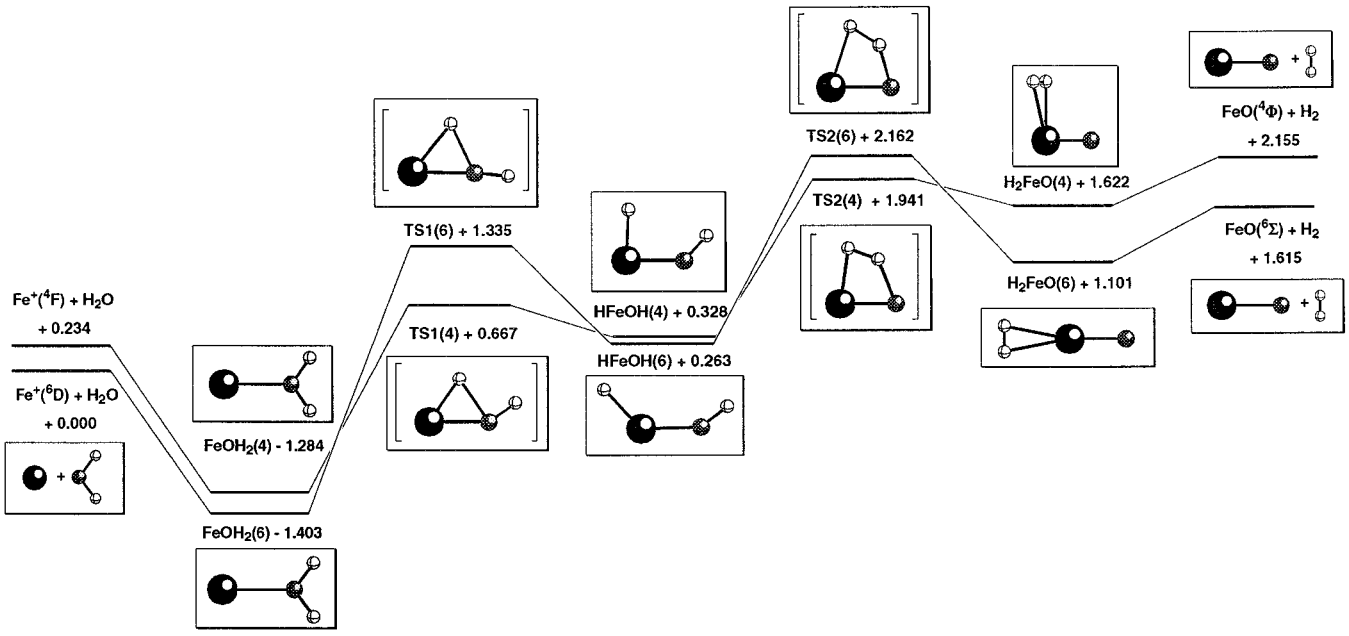

Figure 3. CCSD(T)//B3LYP potential energy surface following the $Fe^+ + OH_2 \rightarrow FeO^+ + H_2$ reaction path. Energies given are in electronvolts and are relative to the separated ground-state reactants, $Fe^+(^6D) + OH_2$. Note that for iron we give this surface rather than the usual B3LYP/DZVP, because the latter is qualitatively misleading.

the sextuplet electromer is calculated to be the ground state; however, the quartet lies only 0.065 eV higher in energy.

The second hydrogen transfer from oxygen to the metal takes place through $TS2^+$. Full agreement is found here, and the sextuplet isomer lies higher in energy than the quartet state. This transition state leads to the final molecular hydrogen metal oxide adduct intermediate found on this reaction path: the (H_2)-FeO^+ ion−molecule complex, whose ground state corresponds once again to a sextet state that is bound by 0.490 eV at the B3LYP/DZVP level of theory, similar to the Cr and Mn values (0.455 eV and 0.407 eV, respectively) for their low-spin ground state $(H_2)MO^+$ moieties. From this intermediate the loss of H_2 proceeds without a transition state to the high-spin MO^+ and H_2.

The dehydrogenation process described here has not been observed experimentally. As was pointed out in the Introduction, Armentrout's group observed only the FeD^+ and $FeOD^+$ products under their conditions. The reverse reaction, however, was observed, and it could follow the path described here. In the $FeO^+ + H_2 \rightarrow Fe^+ + H_2O$ reaction, Clemmer et al.[9] observed a very inefficient barrierless reaction (once in every 600 collisions) and a very efficient reaction with a barrier of

0.6 eV. On our CCSD(T)//B3LYP surface, $TS2^+$ lies 0.547 eV above the separated $FeO^+(^6\Sigma) + H_2$ reactants, and thus the efficient reaction with a barrier is in concurrence with our calculated sextet surface. However, the quartet TS2 also lies higher in energy than $FeO^+(^6\Sigma) + H_2$ (by 0.326 eV), which means that a barrierless pathway, inefficient due to spin crossing, would not agree with our predictions at the CCSD(T)//B3LYP level of theory. At the B3LYP/DZVP and B3LYP/TZVP+G-(3df,2p) levels of theory, the quadruplet $TS2^+$ lies only 0.061 and 0.045 eV above the $FeO^+(^6\Sigma) + H_2$ asymptote in reasonable agreement with the predictions of Filatov and Shaik.[13] In one of the experimental works, it was put forward that perhaps small amounts of $FeO^+(^4\Phi)$ could be in the beam.[9] A later paper, however, dismisses that possibility.[10] At all levels of theory used, the quartet $TS2^+$ lies below the $FeO^+(^4\Phi) + H_2$ asymptote.

Equilibrium geometry parameters for the various reaction products are given in Table 14.

4. Conclusions

The reactions of Cr^+, Mn^+, and Fe^+ with water have been investigated in detail, extending the study of the reactivity of the first-row transition metals. Both the low- and high-spin potential energy surfaces have been characterized at the B3LYP/DZVP and B3LYP/TZVP+G(3df,2p) levels of theory. In addition CCSD(T)//B3LYP single-point energies were computed for many points of interest. From these data, the following conclusions are drawn.

(1) Whereas the only exothermic products of the $M^+ + H_2O$ reaction for M = Sc−V were $MO^+ + H_2$ with exothermicity decreasing from Sc to V, this reaction is endothermic for M = Cr−Fe^+ with endothermicity increasing through the series.

(2) The $Fe^+ + H_2O$ system has proven to be significantly different throughout the reaction pathway. There is less difference between the high- and low-spin structures in the case of Fe^+. An explanation for this is that the high-spin Fe^+ cation has a set of paired electrons while the Sc^+−Mn^+ high-spin cations do not.

(3) Similarly, the high-spin Mn^+ shows some minor differences because its valence shell is completely half-filled with unpaired electrons.

(4) Both high- and low-spin potential energy surfaces cross once in the entrance channel for Cr^+ and Mn^+, but at least two crossings have been observed for the Fe^+ potential energy surface, at the entrance and exit channels. All these crossings occur at an energy *above* that of the ground-state reactants, as was observed earlier in the V potential energy surface.

Acknowledgment. A.I. and J.E.F. thank the Basque Government (Eusko Jaurlaritza) for a grant. Financial support from The University of the Basque Country (Euskal Herriko Unibertsitatea) Grant No. 203.215-G50/98, the Spanish DGICYT Grant No. PB96/1524, and the Provincial Government of Gipuzkoa (Gipuzkoako Foru Aldundia) is gratefully acknowledged. This paper is dedicated to Professor J. Elguero on the occasion of his 65th birthday.

Supporting Information Available: Tables giving total energies for the Cr, Mn, and Fe surfaces (PDF). This material is available free of charge via the Internet at http://pubs.acs.org.

JA984469U